cGAS restricts colon cancer development by protecting intestinal barrier integrity

Shuiqing Hu[a,b], Yan Fang[a,b], Xiang Chen[a,b,c], Tianlei Cheng[a,b], Miaoqing Zhao[d], Mingjian Du[a,b], Tuo Li[a,b,c], Minghao Li[a,b], Zhiqun Zeng[a,b], Yonglong Wei[e], Zhimin Gu[e], Conggang Zhang[a,b], Lijun Sun[a,b], and Zhijian J. Chen[a,b,c,1]

[a]Department of Molecular Biology, University of Texas Southwestern Medical Center, Dallas, TX 75390; [b]Center for Inflammation Research, University of Texas Southwestern Medical Center, Dallas, TX 75390; [c]HHMI, University of Texas Southwestern Medical Center, Dallas, TX 75390; [d]Department of Pathology, Provincial Hospital Affiliated to Shandong First Medical University, 250021 Shandong, China; and [e]Department of Pediatrics, Children's Research Institute, University of Texas Southwestern Medical Center, Dallas, TX 75390

Contributed by Zhijian J. Chen, April 21, 2021 (sent for review March 25, 2021; reviewed by Andrea Ablasser and Jenny P.-Y. Ting)

The DNA-sensing enzyme cyclic guanosine monophosphate-adenosine monophosphate synthase (cGAS) regulates inflammation and immune defense against pathogens and malignant cells. Although cGAS has been shown to exert antitumor effects in several mouse models harboring transplanted tumor cell lines, its role in tumors arising from endogenous tissues remains unknown. Here, we show that deletion of cGAS in mice exacerbated chemical-induced colitis and colitis-associated colon cancer (CAC). Interestingly, mice lacking cGAS were more susceptible to CAC than those lacking stimulator of interferon genes (STING) or type I interferon receptor under the same conditions. cGAS but not STING is highly expressed in intestinal stem cells. cGAS deficiency led to intestinal stem cell loss and compromised intestinal barrier integrity upon dextran sodium sulfate-induced acute injury. Loss of cGAS exacerbated inflammation, led to activation of STAT3, and accelerated proliferation of intestinal epithelial cells during CAC development. Mice lacking cGAS also accumulated myeloid-derived suppressive cells within the tumor, displayed enhanced Th17 differentiation, but reduced interleukin (IL)-10 production. These results indicate that cGAS plays an important role in controlling CAC development by defending the integrity of the intestinal mucosa.

cGAS | STING | inflammation | colon cancer | innate immunity

Colorectal cancer is one of the most common malignant tumors and a leading cause of cancer death for both male and female patients (1). Among multiple factors involved in the initiation and progression of colorectal cancer, inflammation is a major risk factor that drives the development of malignancies in colorectal tissues (2). Patients with inflammatory bowel diseases (IBD) have an increased risk of developing colorectal cancer. Innate immunity has been implicated in maintaining the homeostasis of the gastrointestinal tract and the pathogenesis of IBD as well as IBD-associated colorectal cancer (3).

Cyclic guanosine monophosphate-adenosine monophosphate (cGAMP) synthase (cGAS) is a DNA sensor that triggers innate immune responses (4, 5). Upon DNA binding, cGAS catalyzes the synthesis of the second messenger 2′3′-cGAMP, which in turn binds and activates the endoplasmic reticulum-resident protein stimulator of interferon (IFN) genes (STING). STING activates IκB kinase (IKK) and TANK-binding kinase 1 (TBK1), leading to activation of the transcription factors NF-κB and IRF3, respectively, which then function together to induce the expression of type I IFNs and other immune regulatory molecules (6). cGAS is important for host defense against viral and bacterial infections, but it can also cause autoimmune diseases when it is aberrantly activated by self-DNA. The cGAS-STING pathway has also been shown to play an important role in tumor growth, inflammation, and immune surveillance (7). The activation of the endogenous STING pathway in antigen-presenting cells induces spontaneous T cell priming and antitumor immune responses (8). Intratumoral injection of STING agonists, such as cGAMP or other cyclic dinucleotides, induced the regression of established tumors and also generated a systemic immune response and immunological memory in mouse models of skin, brain, breast, and blood cancers (7, 9). The cGAS-STING pathway is also important for the therapeutic effects of both traditional and new therapies, including radiation, chemicals (e.g., Taxol and PARP inhibitors), and immunotherapies (e.g., antibodies against programmed cell death [PD]-1, PD-L1, and CD47) (10–14). cGAS also regulates cellular senescence to influence tumor growth and development (15–18). However, inflammation induced by the cGAS-STING pathway could also promote tumor growth and metastasis (19–21).

In this study, we investigated the role of cGAS in colon inflammation using a dextran sodium sulfate (DSS)-induced colitis model and colitis-associated colon cancer (CAC) in mice. We found that deletion of cGAS in mice led to severe colitis and CAC. Mice lacking cGAS were more susceptible to CAC than those lacking STING or type I IFN receptor. cGAS shows a specific expression pattern in the colon: expression is the highest in intestinal stem cells and decreases after differentiation. In contrast, STING is highly expressed in the lamina propria and spleen but not in the intestinal stem and epithelial cells. Upon DSS-induced injury, *cGas*$^{-/-}$ but not *Sting*$^{gt/gt}$ mice displayed intestinal stem cell loss and compromised epithelial barrier. cGAS-deficient mice

Significance

Intestinal barrier plays a key role in maintaining organismal health. Here we find cyclic guanosine monophosphate-adenosine monophosphate synthase (cGAS) deficiency compromises intestinal epithelial barrier and exacerbates inflammation. cGAS-deficient mice were highly susceptible to colitis-associated colon cancer (CAC) but not sporadic colon cancer. Surprisingly, the role of cGAS in this process appears to be independent of stimulator of interferon genes (STING)-induced type I interferon signaling, because mice lacking STING or type I interferon receptor were less susceptible to CAC than those lacking cGAS. cGAS but not STING is highly expressed in intestinal stem cells. These results suggest that cGAS has a unique role in protecting the intestinal epithelial barrier and preventing colon cancer development.

Author contributions: S.H. and Z.J.C. designed research; S.H., X.C., and Z.Z. performed research; T.C. contributed new reagents/analytic tools; S.H., Y.F., T.C., M.Z., M.D., T.L., Y.W., Z.G., C.Z., L.S., and Z.J.C. analyzed data; and S.H., Y.F., M.L., and Z.J.C. wrote the paper.

Reviewers: A.A., École Polytechnique Fédérale de Lausanne; and J.P.-Y.T., University of North Carolina at Chapel Hill.

The authors declare no competing interest.

[1]To whom correspondence may be addressed. Email: Zhijian.Chen@UTSouthwestern.edu.

This article contains supporting information online at https://www.pnas.org/lookup/suppl/doi:10.1073/pnas.2105747118/-/DCSupplemental.

Published May 31, 2021.

exhibited elevated inflammatory phenotypes including enhanced STAT3 activation and increased numbers of Th17 cells, which together exacerbate colonic inflammation, cellular proliferation, and tumorigenesis. Administration of STAT3 inhibitor or cGAMP partially inhibited colorectal cancer development in cGAS-deficient mice. These results suggest that cGAS suppresses colon inflammation and tumorigenesis by defending the intestinal mucosal barrier.

Results

cGAS Protects Mice from DSS-Induced Colitis. To assess the function of cGAS in the intestine, we fed the *cGas*$^{-/-}$ and WT mice with 3% DSS in drinking water for 5 d to induce acute colitis (Fig. 1*A*). This chemical-induced colitis model has been shown to recapitulate many of the clinical features associated with ulcerative colitis (22). Colitis susceptibility was evaluated daily by monitoring body weight changes and clinical features of colitis, such as diarrhea and occult stool bleeding. *cGas*$^{-/-}$ mice lost significantly more body weight and exhibited increased diarrhea and rectal bleeding compared to WT mice (Fig. 1 *B–D*). Mice were killed on day 8 and examined for histopathological changes. *cGas*$^{-/-}$ mouse colons were significantly shorter than those in the WT mice (Fig. 1 *E* and *F*). The severity of colitis in *cGas*$^{-/-}$ mice was further supported by histological staining of whole colon tissue sections (Fig. 1*G*). Compared to WT mice, much of the distal colon in *cGas*$^{-/-}$ mice showed increased severity of disease with complete crypt destruction, epithelium ulceration, and submucosal edema (Fig. 1*G*). Histopathological analysis showed significantly higher scores for inflammation, ulceration, and crypt distortion in *cGas*$^{-/-}$ mouse colons (Fig. 1*H*). These data suggest a protective role for cGAS in acute colitis induced by DSS.

cGAS Restricts CAC. Patients with IBD are at a higher risk of colorectal cancer (2). We further explored the role of cGAS in the development of IBD-associated colon tumorigenesis by using azoxymethane (AOM) as a carcinogen in the DSS-induced inflammation-driven colon cancer model (Fig. 2*A*) (23, 24). Following initial injection with AOM and three cycles of 1.5% DSS treatments, *cGas*$^{-/-}$ mice developed significantly increased numbers of macroscopic colon tumors throughout the whole colon, including proximal, middle, and distal colon (Fig. 2 *B* and *C*), while only several scattered tumors appeared mainly in the distal colon of

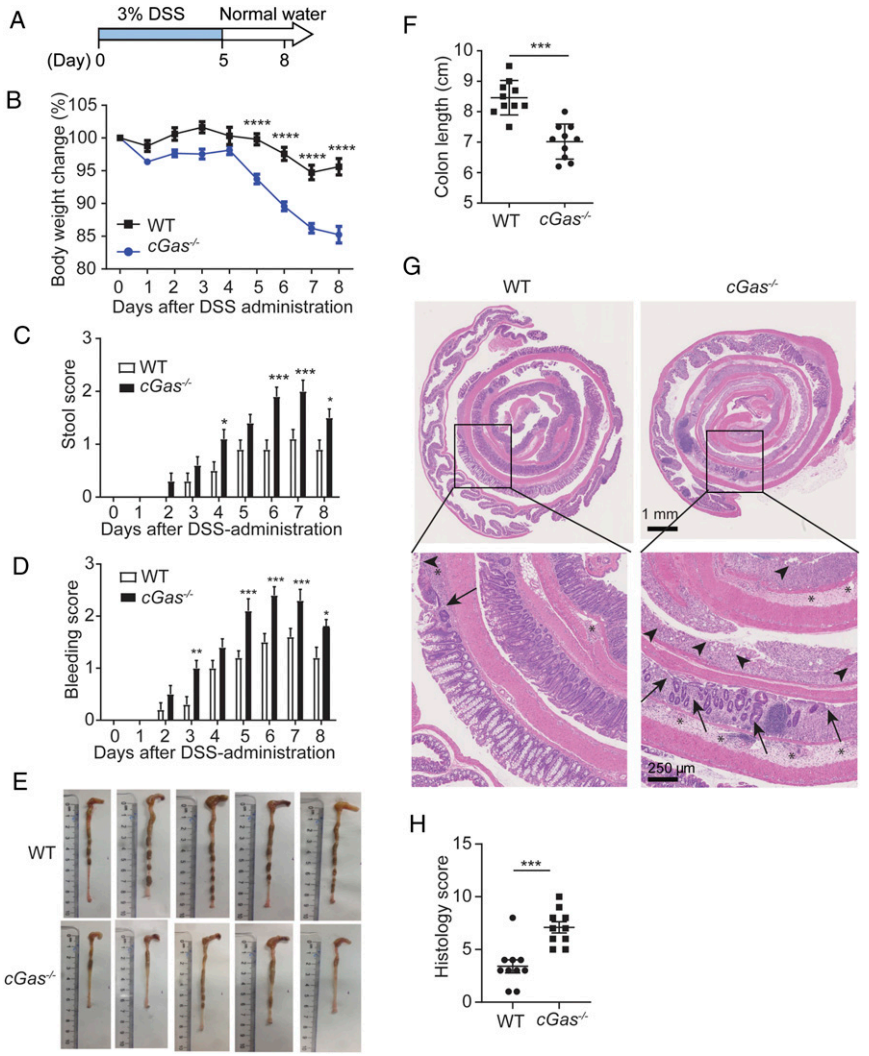

Fig. 1. *cGas*$^{-/-}$ mice are susceptible to DSS-induced colitis. WT and *cGas*$^{-/-}$ mice ($n = 10$ per group) were fed with 3% DSS in water for 5 d, followed by regular drinking water for additional 3 d. (*A*) Schematic of DSS-induced colitis model. (*B–D*) Body weight (*B*), stool consistency (*C*), and rectal bleeding (*D*) were scored daily. (*E* and *F*) Colon lengths were measured and representative pictures on day 8 are shown. (*G*) Colon tissues collected on day 8 after DSS administration were stained with H&E. Crypt loss or destruction (arrows), epithelial ulceration (arrowheads), and severe edema (asterisks) are indicated. (*H*) Semiquantitative scoring of histopathology was performed. $^{*}P < 0.05$; $^{**}P < 0.01$; $^{***}P < 0.001$; $^{****}P < 0.0001$.

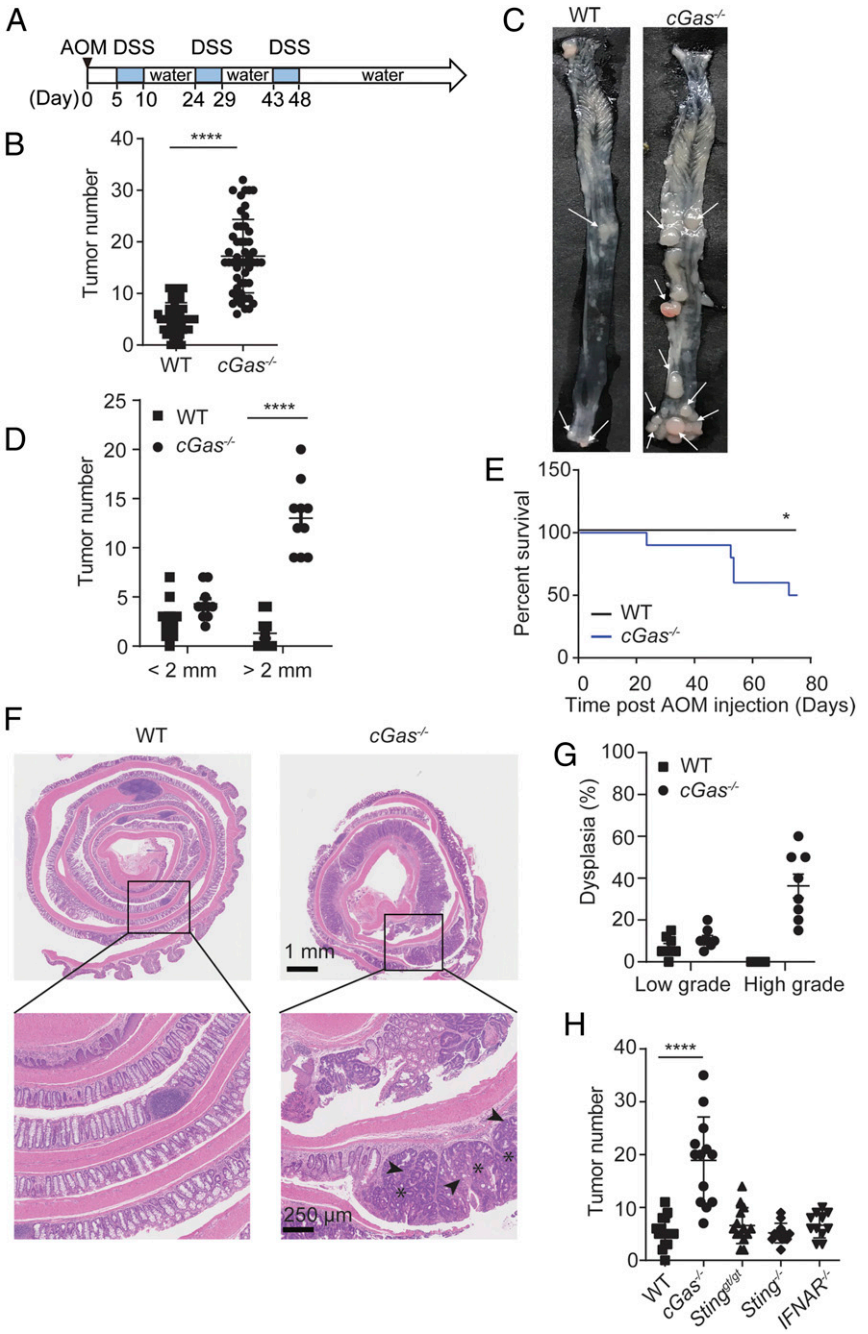

Fig. 2. Deletion of cGAS promotes colitis-associated tumor formation. (*A*) The schematic of AOM/DSS-induced colitis-associated tumor formation model. WT and *cGas*$^{-/-}$ mice were intraperitoneally injected with 8 mg/kg AOM on day 0 and then given 1.5% DSS solution on day 5 for 5 d followed by regular drinking water for 2 wk, and the cycle was repeated twice. (*B*) The number of tumors in the whole colon was counted at the end of the study. Experiments were repeated five times and combined results ($n = 50$ per group) are shown. (*C*) Representative pictures of colon tumor development in WT and *cGas*$^{-/-}$ mice. Arrows indicate tumors. (*D*) The number of mice bearing tumors of different diameters was calculated. (*E*) The survival of mice treated with AOM and 2.5% DSS was monitored throughout the study and the Mantel–Cox test was performed. (*F*) Representative H&E-stained images of the colon tissues. High-grade dysplasia (asterisk) and adenocarcinoma (arrowheads). (*G*) The percentage of dysplasia on day 80 by histological analysis. (*H*) WT ($n = 16$), *cGas*$^{-/-}$ ($n = 13$), *Sting*$^{gt/gt}$ ($n = 14$), *Sting*$^{-/-}$ ($n = 12$), and *IFNAR*$^{-/-}$ ($n = 11$) mice were intraperitoneally injected with 8 mg/kg AOM and given three cycles of 1.5% DSS for colon cancer induction. The number of tumors in the whole colon was counted at the end of the study. *$P < 0.05$; ****$P < 0.0001$.

WT mice. The sizes of macroscopic tumors (maximal cross-sectional area of tumors >2 mm) were greatly increased in *cGas*$^{-/-}$ mice compared to WT controls (Fig. 2*D*). However, colon lengths were similar between WT and *cGas*$^{-/-}$ mice (*SI Appendix*, Fig. S1*A*). In addition, we found that around 50% *cGas*$^{-/-}$ mice died early, whereas WT mice survived when given 2.5% DSS water (Fig. 2*E*). *cGas*$^{-/-}$ mice also showed splenomegaly and heavier spleen weight compared to WT mice after CAC development (*SI Appendix*, Fig. S1 *B* and *C*), while both WT and *cGas*$^{-/-}$ spleens in untreated animals had similar weights (*SI Appendix*, Fig. S1*D*).

Histopathological analyses showed that *cGas*$^{-/-}$ mice exhibited increased hyperplasia in the proximal, middle, and distal colon, while WT mice showed none or much less hyperplasia in the distal colon (Fig. 2*F*). Low-grade colonic mucosal dysplasia

was observed in tumor-bearing WT mice, whereas low-grade to high-grade dysplasia was found in *cGas*$^{-/-}$ mice (Fig. 2 *F* and *G*). Histological analysis also showed more adenocarcinomas in cGAS-deficient mice than in WT mice (Fig. 2*F*), suggesting the absence of cGAS accelerates tumor progression. However, we did not observe submucosal invasion of tumor cells in *cGas*$^{-/-}$ mice, indicating that cGAS deficiency did not impact metastasis in the CAC model. Interestingly, mice lacking STING (*Sting*$^{gt/gt}$ and *Sting*$^{-/-}$) or type I IFN receptor (*IFNAR*$^{-/-}$) did not show a significant increase of colon tumors in this DSS-AOM model, suggesting that cGAS restricts colon cancer development through a mechanism that is independent of STING or type I IFN signaling (Fig. 2*H*).

The microbiota is widely reported to regulate the pathogenesis and severity of gastrointestinal diseases, including CAC. 16S rRNA analysis showed similar levels of several known mouse gut commensal and colitogenic bacteria, such as *Bacteroides*, *Lactobacillus*, segmented filamentous bacteria, *Staphylococcus*, *Streptococcus*, *Escherichia coli*, *Enterococcus*, and Bifidobacteria, between WT and *cGas*$^{-/-}$ mice (*SI Appendix*, Fig. S1*E*). To further explore the role of microbiota, WT and *cGas*$^{-/-}$ mice were cohoused for 4 wk before inducing colon cancer. Similar to single-housed mice, cohoused *cGas*$^{-/-}$ mice also had higher tumor numbers than cohoused WT mice (*SI Appendix*, Fig. S1*F*). In addition, examination of the littermates from breeding of cGAS heterozygous mice showed *cGas*$^{-/-}$ mice also had significantly more tumor numbers than WT mice (*SI Appendix*, Fig. S1*G*). Importantly, *cGas*$^{-/-}$ mice pretreated with antibiotics developed similar tumor numbers to those in the *cGas*$^{-/-}$ mice without antibiotic treatment; but the tumor numbers in both *cGas*$^{-/-}$ mice were more than those in the WT mice that were pretreated with antibiotics (*SI Appendix*, Fig. S1*H*). These results indicate that the microbiota is not a key determinant for accelerated tumor development in the *cGas*$^{-/-}$ mice.

Colorectal cancers develop either spontaneously or as a complication of IBD. As cGAS prevents colitis-associated colon tumorigenesis, we further explored whether cGAS is also involved in sporadic colon cancer using the *Apc*$^{min/+}$ mouse, a noncolitis-driven colorectal cancer model (25). Mutations of the APC gene, which normally inhibits the Wnt/β-catenin pathway, accelerates colorectal tumorigenesis in mice and humans. We analyzed sex- and age-matched cohorts of *Apc*$^{min/+}$ mice on cGAS-sufficient and -deficient backgrounds. *cGas*$^{-/-}$*Apc*$^{min/+}$ mice had similar numbers of colon tumors as *cGas*$^{+/+}$*Apc*$^{min/+}$ mice (*SI Appendix*, Fig. S1*I*). Although *cGas*$^{+/+}$*Apc*$^{min/+}$ mice had high numbers of tumors in the small intestine, *cGas*$^{-/-}$*Apc*$^{min/+}$ mice

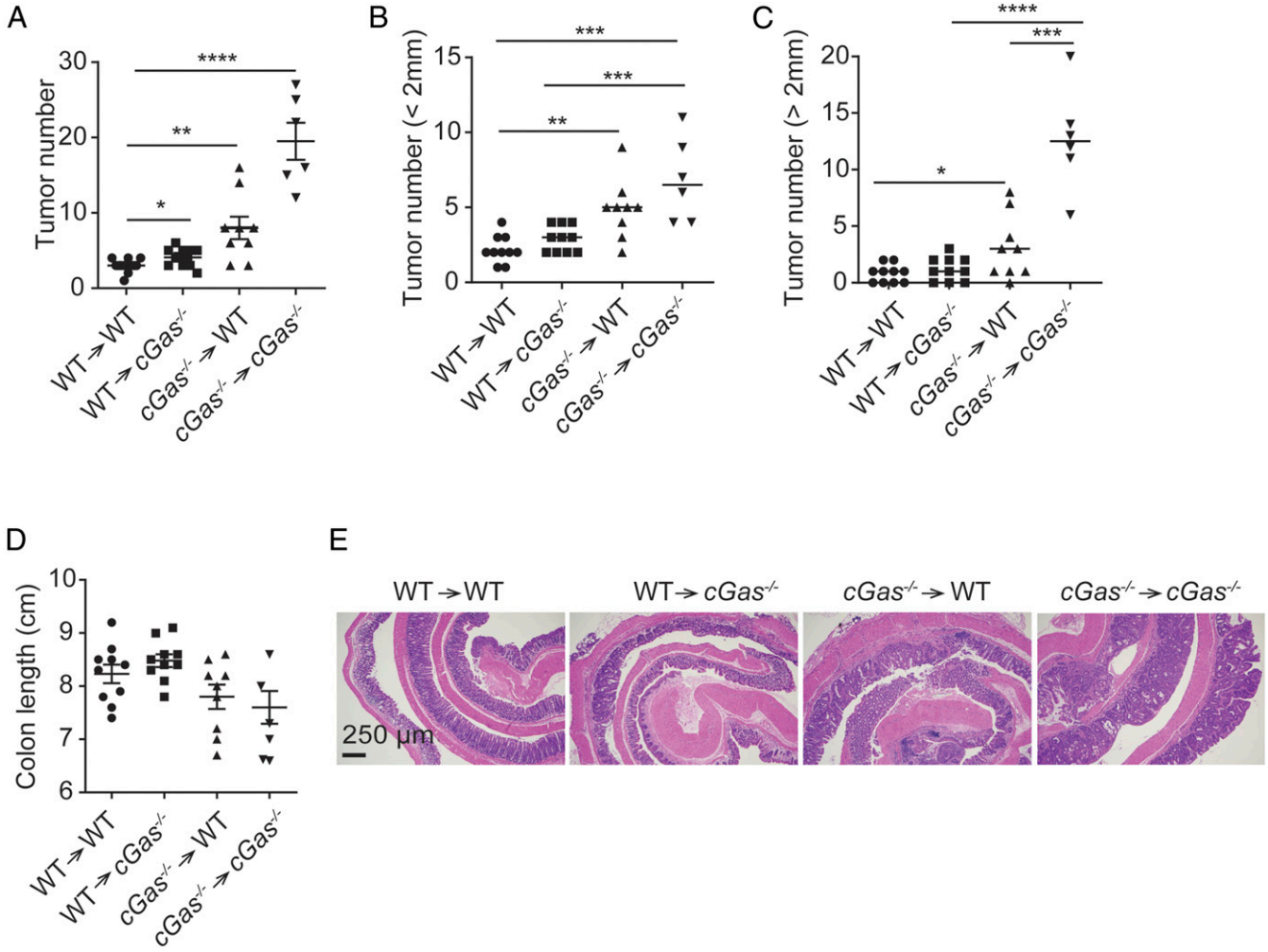

Fig. 3. cGAS signaling in both hematopoietic and nonhematopoietic cells contributes to protection against colon cancer development. (*A*–*C*) Four groups of mice were generated by bone marrow transplantation: 1) WT→WT ($n = 10$); 2) *cGas*$^{-/-}$→WT ($n = 9$); 3) WT→*cGas*$^{-/-}$ ($n = 10$); 4) *cGas*$^{-/-}$→*cGas*$^{-/-}$ ($n = 10$, 4 died during experiment). Eight weeks following bone marrow transplantation, mice were treated with AOM followed by three cycles of 1.5% DSS, and colon tumors were counted 80 d after injection of AOM. The number of tumors in the colon with different sizes were quantified. (*D*) The colon lengths in different groups were measured. (*E*) Representative H&E images of colon tumors. Each symbol in the graph represents one mouse. *$P < 0.05$; **$P < 0.01$; ***$P < 0.001$; ****$P < 0.0001$.

did not show obvious changes in overall tumor numbers compared to $cGas^{+/+}Apc^{min/+}$ mice (*SI Appendix*, Fig. S1*J*). Altogether, these results suggest that cGAS does not restrict sporadic colon tumorigenesis, but inhibits CAC.

cGAS in Both Hematopoietic and Nonhematopoietic Cells Regulates CAC. To identify the cellular source responsible for the enhanced tumorigenesis in the absence of cGAS, we performed bone marrow transplantation experiments to examine the contribution of the radio-resistant nonhematopoietic compartment relative to that of the radio-sensitive hematopoietic compartment by generating bone marrow-chimeric mice. WT and $cGas^{-/-}$ mice were exposed to whole-body irradiation to deplete hematopoietic stem cells and progenitor compartments. Irradiated recipients were then injected with either WT or $cGas^{-/-}$ bone marrow. After 2-mo reconstitution with an efficiency around 90%, CAC was induced with AOM and DSS, as described above. WT mice reconstituted with $cGas^{-/-}$ bone marrow ($cGas^{-/-}$→WT) exhibited increased tumor sizes and number as compared to WT control mice (WT→WT) (Fig. 3 *A*–*C*). In contrast, $cGas^{-/-}$ recipient mice reconstituted with WT bone marrow (WT→$cGas^{-/-}$) had significantly lower tumor burden than mice lacking cGAS in both compartments ($cGas^{-/-}$→$cGas^{-/-}$), suggesting that cGAS expression in the hematopoietic compartment plays a major role in the restriction of tumorigenesis during CAC (Fig. 3 *A*–*C*). However, the WT→$cGas^{-/-}$ group still had increased colon tumor loads as compared to the WT→WT controls (Fig. 3*A*), and the $cGas^{-/-}$→WT group exhibited significantly smaller tumor sizes and lower numbers compared to the $cGas^{-/-}$→ $cGas^{-/-}$ group (Fig. 3 *A*–*C*), indicating that cGAS expression in radio-resistant, nonhematopoietic cells also limits tumorigenesis during CAC. Colon lengths did not show significant statistical differences among different groups (Fig. 3*D*). Histopathology analyses further confirmed that cGAS expression in both hematopoietic and nonhematopoietic compartments contribute to CAC development (Fig. 3*E*). Altogether, these results suggest that cGAS protects colon cancer development in both hematopoietic and nonhematopoietic compartments.

cGAS Controls CAC by Regulating the Intestinal Epithelial Barrier and Enterocyte Proliferation. To assess cGAS function in CAC, we investigated cGAS expression in the intestinal crypts that contain stem cells and differentiated intestinal epithelial cells (IECs), lamina propria cells, colons, and spleens. Interestingly, cGAS expression was much higher in the crypts than in the lamina propria cells and splenocytes. In contrast, STING expression was much higher in splenocytes and lamina propria cells than in crypts (Fig. 4*A*). These results suggest a cGAS-dependent but STING-independent function in crypts. By analyzing published single-cell RNA-sequencing (scRNA-seq) data by Haber et al. (26), we found that cGAS (Mb21d1) expression was the highest in the intestinal stem cell ($Lgr5^+$) population. The expression of cGAS was gradually down-regulated during differentiation with medium expression levels in early differentiated cells, such as transient amplifying cells and enterocyte progenitors, and low expression level in terminal differentiated cells, such as enterocytes, paneth cells, and goblet cells (Fig. 4*B*).

Consistent with these results, analysis of the published scRNA-seq data from Ayyaz et al. (27) showed that the intestinal stem cells expressed much higher levels of cGAS RNA than myeloid cells and lymphocytes (*SI Appendix*, Fig. S2*A*). However, STING (Tmem173) was highly expressed in immune cells but not in IECs (Fig. 4*B* and *SI Appendix*, Fig. S2*A*). Importantly, by analyzing cells from Lgr5-EGFP reporter mice, we found that cGAS expression was higher in the $Lgr5^+$ populations compared to the Lgr5dim and spleen cell population, whereas STING expression was higher in the spleen but lower in the $Lgr5^+$ and Lgr5dim populations (Fig. 4*C*). Together, these results suggest that cGAS may regulate intestinal stem cells through a STING-independent mechanism. While Lgr5 expression was initially comparable between WT and $cGas^{-/-}$ mice, AOM and DSS treatment decreased Lgr5 expression in the crypts of $cGas^{-/-}$ mice, whereas the levels of Lgr5 expression were largely unchanged in WT and $Sting^{gt/gt}$ mice (Fig. 4 *D* and *E*). The results suggest that cGAS, but not STING, plays a critical role in regulating intestinal stem cells in the crypts. As the epithelial barrier controls intestinal homeostasis, we also investigated intestinal barrier integrity during the acute inflammation phase after AOM/DSS treatment. Compared to WT and $Sting^{gt/gt}$ mice, significantly more FITC-dextran was found in the serum of $cGas^{-/-}$ mice after DSS-induced injury (Fig. 4*F* and *SI Appendix*, Fig. S2*B*). No difference in FITC-dextran concentrations was observed between $cGas^{-/-}Apc^{min/+}$ and $cGas^{+/+}Apc^{min/+}$ mice (*SI Appendix*, Fig. S1*K*). These results indicate that cGAS protects gastrointestinal barrier integrity to prevent CAC.

To further investigate the mechanism by which the loss of cGAS exacerbates CAC development, we examined whether cGAS regulates cellular proliferation following exposure to AOM and DSS. Immunohistochemical analyses at 80 d after injection of AOM revealed significantly higher numbers of K_i67^+ cells per crypt in the intestinal epithelium of $cGas^{-/-}$ mice than in WT mice (Fig. 4*G*), whereas no difference was observed in untreated WT and $cGas^{-/-}$ mice (*SI Appendix*, Fig. S2*C*). These results suggest that cGAS deficiency led to faster proliferation of IECs during cancer development. Consistently, we also found a significantly higher number of $BrdU^+$ cells per crypt in the colons of $cGas^{-/-}$ mice at 80 d after injection of AOM (Fig. 4*H*), with similar low incorporation numbers for the untreated WT and $cGas^{-/-}$ mice (*SI Appendix*, Fig. S2*D*). The tumor areas of $cGas^{-/-}$ mice showed even more K_i67^+ and $BrdU^+$ cells (*SI Appendix*, Fig. S2*E*). S100a9 was reported to be an important proinflammatory mediator in colonic inflammation and contributed to tumorigenic processes by regulating cell proliferation (28). Real-time PCR analysis found that the levels of S100a9 RNA in the colon of $cGas^{-/-}$ mice at 15 and 80 d after injection of AOM were higher than those in WT mice (Fig. 4*I*).

Increased intestinal cell proliferation may be related to reduced apoptosis. However, the RNA levels of the antiapoptotic gene Bcl-2 in the colon did not show a significant difference between WT and $cGas^{-/-}$ mice on days 15 and 80 after injection of AOM, while the apoptotic gene Bax in the colon of $cGas^{-/-}$ mice increased on day 80 (*SI Appendix*, Fig. S3*A*). Moreover, apoptotic caspase-7 and caspase-3 cleavage in the colon of $cGas^{-/-}$ mice was stronger than that in WT mice on day 80 (*SI Appendix*, Fig. S3*B*), suggesting more cell death in $cGas^{-/-}$ mice during CAC development. Terminal deoxynucleotidyl transferase dUTP nick end-labeling (TUNEL) staining of colon sections also revealed accelerated apoptosis in $cGas^{-/-}$ mice, especially within the tumor (Fig. 4*J* and *SI Appendix*, Fig. S3*C*). There was also more $TUNEL^+$ staining in $cGas^{-/-}$ mice during acute colitis (*SI Appendix*, Fig. S3 *D* and *E*). It's possible that the enhanced apoptosis of IECs in $cGas^{-/-}$ mice led to compensatory hyperproliferation of these cells, which contributes to colon tumor development in $cGas^{-/-}$ mice.

To examine possible intrinsic defects in the mucus layer, we analyzed whether cGAS regulates the expression of genes encoding mucins in the colon. The expression of MUC2, MUC3, and MUC4 in the colon of WT and $cGas^{-/-}$ mice were comparable in untreated animals. After the AOM/DSS treatment, although only Muc2 RNA levels showed a lower expression in the $cGas^{-/-}$ mice than in the WT mice on day 15, the RNA levels of Muc2, Muc3, and Muc4 all decreased on day 80 in the colon of $cGas^{-/-}$ mice compared to those of WT mice (*SI Appendix*, Fig. S3*F*). In contrast to mucin genes, the expression levels of tight junction genes ZO-1, ZO-2, and occludin were similar in the crypts between WT and $cGas^{-/-}$ mice on day 80 after the AOM/DSS treatment (*SI Appendix*, Fig. S3*G*). The decreased expression of the mucin genes in the $cGas^{-/-}$ mice may contribute to the leaky intestinal barrier in these mice.

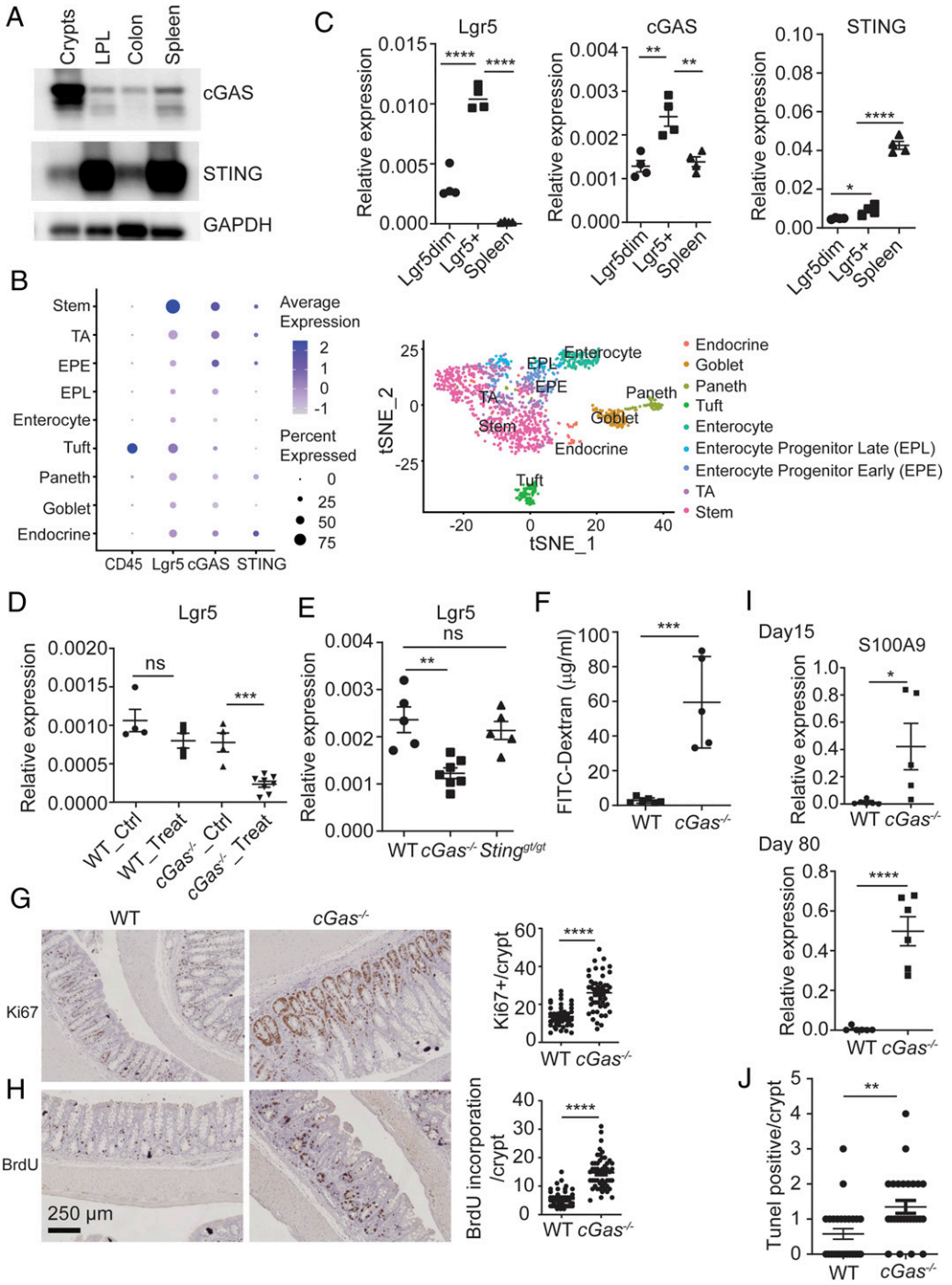

Fig. 4. cGAS deficiency enhances proliferation of the intestinal epithelium and permeabilization of the intestinal barrier. (*A*) The expression of cGAS and STING in the crypts, lamina propria, colon, and spleen was measured by Western blotting. (*B*) Reanalysis of the scRNA-seq data by Haber et al. (26). t-SNE of scRNA-seq dataset from 1,522 epithelial cells. Cell types were determined based on annotation in the original paper. The fraction of each cell type expressing target genes (size of dot) and the expression levels of each gene in those expressing cells (color bar) are shown. Mann–Whitney *U* test was used for analysis. (*C*) Lgr5^{+} and Lgr5dim cells were isolated as described in *Materials and Methods*. The expression of cGAS, STING, and Lgr5 in the indicated groups were analyzed by qRT-PCR. (*D*) Lgr5 RNA levels in the crypts of WT and *cGas*$^{-/-}$ mice that were either untreated or treated with AOM/DSS for 15 d. (*E*) Lgr5 RNA levels in the crypts of WT, *cGas*$^{-/-}$, and *Sting*$^{gt/gt}$ mice on day 15 after treatment with AOM/DSS. (*F*) After AOM injection, WT ($n = 6$) and *cGas*$^{-/-}$ mice ($n = 5$) were fed with 2.5% DSS solution for 5 d, followed by regular drinking water for 5 d. Mice were subsequently fed FITC-dextran by oral gavage, and FITC-dextran concentrations in the sera were determined. (*G*) Mouse colon tumors were induced as described in Fig. 2. The colon tissues were stained with an antibody against K_i67 and the number of K_i67^{+} cells in each crypt was quantified. (*Left*) Representative images of K_i67 staining in the colon crypts. (*Right*) Quantification of the number of K_i67^{+} cells in the colon crypts of WT ($n = 5$) and *cGas*$^{-/-}$ mice ($n = 6$) on day 80 after AOM injection. (*H*) BrdU was intraperitoneally injected 2 h before the mice were killed. The colon tissues were stained using the BrdU In-Situ Detection Kit. (*Left*) representative images of BrdU staining in the colon crypts. (*Right*) Quantification of the number of BrdU^{+} cells in each crypt of WT and *cGas*$^{-/-}$ ($n = 5$ each group) mice on day 80 after AOM injection. (*I*) qRT-PCR analysis of S100A9 gene in WT and *cGas*$^{-/-}$ mice on day 15 and 80 after injection of AOM. (*J*) TUNEL staining of colon tissues of mice on day 80 after injection of AOM. *$P < 0.05$; **$P < 0.01$; ***$P < 0.001$; ****$P < 0.0001$; ns, not significant.

cGAS Deficiency Led to Enhanced Activation of STAT3, but Not Type I IFNs. To investigate the molecular mechanism underpinning cGAS-dependent protection against colorectal tumorigenesis, we examined whether there was a defect in type I IFN signaling in *cGas*$^{-/-}$ mice during colon cancer development, as the function of cGAS in infection and autoimmunity depends on the production of type I IFN. Similarly low levels of IFN-α and IFN-β in the colon were detected in untreated WT and *cGas*$^{-/-}$ mice (*SI Appendix*, Fig. S4*A*). We then analyzed IFN-α and IFN-β production in the whole colon of WT and *cGas*$^{-/-}$ mice at 15 d after injection of AOM and found similar levels of type I IFN production in the early stage of CAC (*SI Appendix*, Fig. S4*B*). The production of type I IFN in the whole colon also showed no overt differences between WT and *cGas*$^{-/-}$ mice on day 80 when the colon cancer had reached the advanced stage (*SI Appendix*, Fig. S4*B*). IFN-β levels in the serum on days 15 and 80 were also comparable between WT and *cGas*$^{-/-}$ mice (*SI Appendix*, Fig. S4*C*). IFNAR1 expression in the CD11b^{+} and CD11b^{+}F4/80^{+} populations in the colon also showed similar levels between WT and *cGas*$^{-/-}$ mice (*SI Appendix*, Fig. S4*D*). Similar gene-expression levels of IFN-stimulated genes (ISGs)—including CXCL10, ISG15, and IFIT3—were observed in the colon tissues of WT and

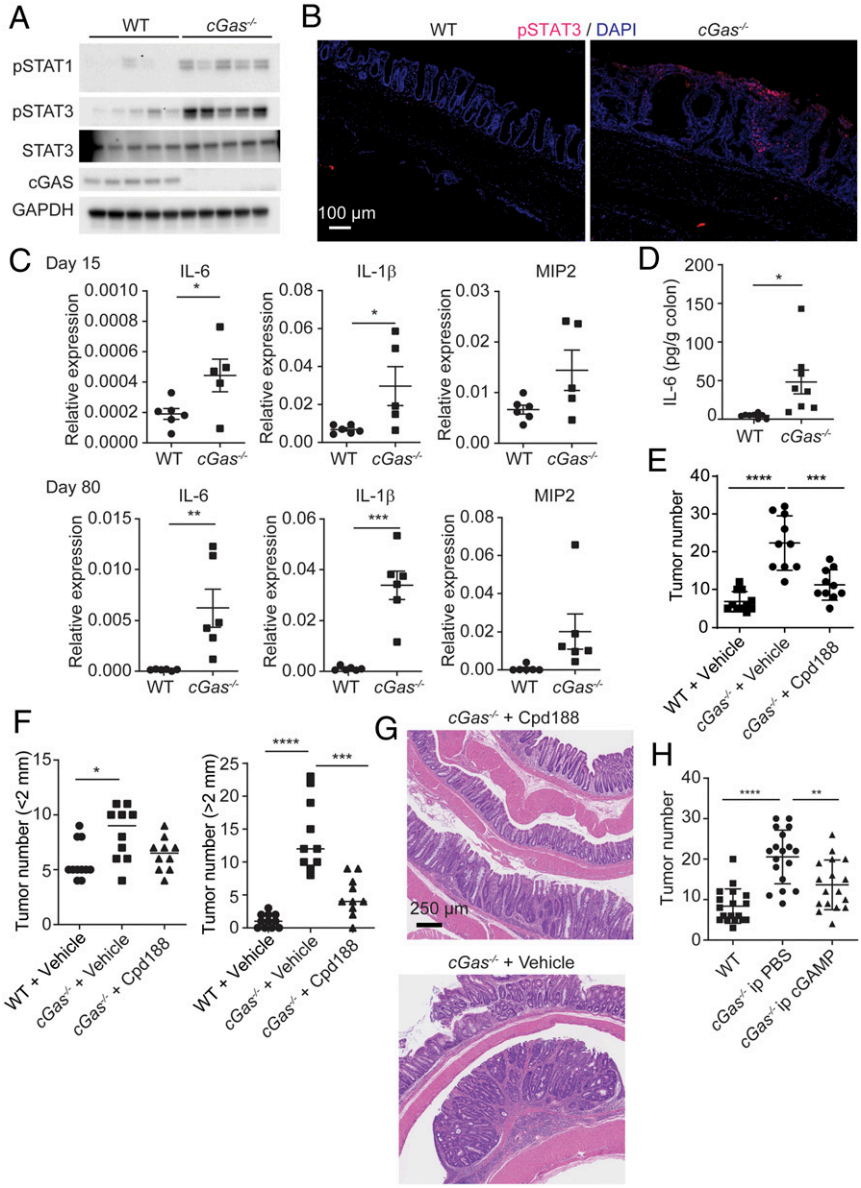

Fig. 5. STAT3 is activated in the colon of cGAS-deficient mice mouse colon tumors were induced as described in Fig. 2. WT and *cGas*$^{-/-}$ colons and sera were collected on day 15 and 80 after AOM injection. (*A*) Western blot analysis of the indicated proteins in the colons isolated from the mice on day 80 after initiation of the AOM/DSS treatment ($n = 5$ each group). (*B*) Immunostaining of phosphorylated STAT3 (red) in colon tissues isolated from mice on day 80 after treatment initiation. DAPI stains DNA (blue). (*C*) qRT-PCR analyses of the indicated cytokine genes in colon tissues from WT and *cGas*$^{-/-}$ mice on days 15 and 80 after injection of AOM. (*D*) Whole colon homogenates were quantified for IL-6 expression by ELISA. (*E*) The STAT3 inhibitor Cpd188 or vehicle (0.8% DMSO) was intraperitoneally injected into mice during the recovery phase of DSS challenge every 2 or 3 d until the end of the study and the numbers of tumors in the whole colon were counted. WT ($n = 11$), *cGas*$^{-/-}$ + Vehicle ($n = 10$), and *cGas*$^{-/-}$ + Cpd188 ($n = 10$). (*F*) The different sizes of tumors in the Cpd188 and vehicle-treated groups were determined. (*G*) Histological analysis of colons in the Cpd188 and vehicle-treated mice. (*H*) cGAMP (30 μg) was intraperitoneally injected into *cGas*$^{-/-}$ mice during the recovery phase of DSS challenge every 2 or 3 d until the end of the study and the numbers of macroscopic colon tumors were counted. WT ($n = 18$), *cGas*$^{-/-}$ + PBS ($n = 18$), and *cGas*$^{-/-}$ + cGAMP ($n = 17$). *$P < 0.05$; **$P < 0.01$; ***$P < 0.001$; ****$P < 0.0001$.

cGas$^{-/-}$ mice at 15 d after injection of AOM, but the expression of CXCL10 and ISG15 was even higher in *cGas*$^{-/-}$ mice at 80 d after injection of AOM (*SI Appendix*, Fig. S4*E*). cGAS expression level in the whole colon was also not altered at days 15 and 80 after injection of AOM (*SI Appendix*, Fig. S4*F*). We further analyzed colon STAT1 phosphorylation, a hallmark of type I IFN pathway activation. *cGas*$^{-/-}$ mice showed higher levels of STAT1 phosphorylation in the colon compared to WT mice on days 15 and 80 (Fig. 5*A* and *SI Appendix*, Fig. S5*A*). Altogether, these results suggest no apparent defect in type I IFN signaling in the colons of *cGas*$^{-/-}$ mice compared to WT mice during CAC; instead, type I IFN signaling appeared to be enhanced at the later stage of CAC in the *cGas*$^{-/-}$ mice.

STAT3 activation has been implicated in driving colon cancer development in both CRC patients and mouse colon tumor models (29, 30). We found by Western blotting that on days 15 and 80 the phosphorylation of STAT3 in the colon was stronger in *cGas*$^{-/-}$ mice than in WT mice (Fig. 5*A* and *SI Appendix*, Fig. S5*A*). Immunohistology staining further confirmed higher phosphorylation of STAT3 in the colon of *cGas*$^{-/-}$ mice on day 80 (Fig. 5*B*). Even in the acute colitis model induced by DSS, the colon of *cGas*$^{-/-}$ mice showed stronger phosphorylation of STAT3 than WT mice on day 8 after treatment (*SI Appendix*, Fig. S5*A*). *Apc*$^{min/+}$ displayed high levels of STAT3 phosphorylation in the colon (31). However, cGAS deficiency did not further affect STAT3 phosphorylation in the *Apc*$^{min/+}$ mice (*SI Appendix*, Fig. S5*B*). In addition, we found that mRNA levels of interleukin (IL)-6, IL-1β, and MIP2 in the whole colon were significantly higher in the *cGas*$^{-/-}$ mice bearing colon tumors (Fig. 5*C*). Higher levels of IL-6 protein in the colon of *cGas*$^{-/-}$ mice were further detected by ELISA, suggesting that IL-6–STAT3 signaling may be important for the CAC in the *cGas*$^{-/-}$ mice (Fig. 5*D*). Using MC38 colon cancer cell lines, we found IL-6–induced STAT3 phosphorylation was not impaired by cGAS deficiency, but was blocked by an anti–IL-6 antibody or the STAT3 inhibitor Cpd188 (*SI Appendix*, Fig. S5*C*) (32). These results indicate that the enhanced phosphorylation of STAT3 observed in the colon tissues of *cGas*$^{-/-}$ mice was not due to increased sensitivity to IL-6 stimulation but increased production of IL-6 and other inflammatory cytokines.

WT and cGAS-deficient bone marrow-derived macrophages (BMDMs) showed similar levels of phosphorylation of IκBα and ERK1/2 after treatment with tumor necrosis factor-α (TNF-α) or the ligands for Toll-like receptor (TLR)4 and TLR2 (*SI Appendix*, Fig. S5*D*). Both AIM2- and NLRP3-inflammasome activation played a protective role in regulating colon inflammation and cancer development (33–35). Compared to WT BMDMs, *cGas*$^{-/-}$ BMDMs showed similar activation of AIM2 and NLRP3 inflammasomes upon stimulation with double-stranded DNA and nigericin, respectively (*SI Appendix*, Fig. S5*E*). The DNA from mouse stool could also induce similar inflammasome activation in WT and *cGas*$^{-/-}$ BMDMs (*SI Appendix*, Fig. S5*E*). These results suggest that the enhanced CAC development in *cGas*$^{-/-}$ mice was not due to aberrant inflammasome activation.

To further explore whether STAT3 activation promotes colon cancer development in *cGas*$^{-/-}$ mice, we treated colon cancer-bearing mice with the STAT3 inhibitor Cpd188 intraperitoneally (32). At the end of the treatment period, tumor numbers in the Cpd188-treated group decreased as compared with vehicle-treated group (*SI Appendix*, Fig. S5*E*). The sizes of tumors in the Cpd188 treated group were also smaller than those of vehicle-treated mice (Fig. 5*F*). No gross toxicities were evident as determined by the change of body weight. Histological analysis showed that low inflammation and dysplasia was observed for the Cpd188-treated group, while severe inflammation and high dysplasia were found in the vehicle-treated group (Fig. 5*G*). These results suggest that STAT3 activation in the *cGas*$^{-/-}$ mice promoted colon cancer development.

cGAMP Treatment Partially Inhibits CAC. The cGAS product cGAMP has been shown to exert strong antitumor effects in several mouse models bearing transplanted tumor cell lines (12). However, the effect of cGAMP on tumors arising from endogenous tissues has not been reported. The aggressive development of colon cancers induced by DSS and AOM in the *cGas*$^{-/-}$ mice offers an opportunity to test the effect of cGAMP on endogenous tumors. In vitro stimulation with cGAMP could induce IFN-β and CXCL10 expression in both WT and cGAS-deficient BMDM (*SI Appendix*, Fig. S6*A*). Intraperitoneal injection of cGAMP could also induce IFN-α and IFN-β production in the crypts and spleen of *cGas*$^{-/-}$ mice, indicating that cGAMP intraperitoneal administration induces not only local activation, but also systemic responses (*SI Appendix*, Fig. S6*B*). These results suggest that cGAMP might have potential therapeutic effects for colon cancer treatment of *cGas*$^{-/-}$ mice. cGAMP was injected to mice intraperitoneally during the recovery phase of the DSS treatment cycle (*SI Appendix*, Fig. S6*C*). This treatment partially but significantly reduced the number of tumors in the colon when compared to untreated mice (Fig. 5*H*), providing evidence that cGAMP has therapeutic potential in tumors arising from an internal organ. The sizes of tumors were smaller and histological study showed lower dysplasia in cGAMP-treated *cGas*$^{-/-}$ mice than PBS-treated mice (*SI Appendix*, Fig. S6 *D* and *E*).

Dysregulation of T Cells in *cGas*$^{-/-}$ Mice during Colon Cancer Development. T cell dysfunction is implicated in regulating colonic cancer development. Although there was a similar percentage of $CD3^+CD4^+$ and $CD3^+CD8^+$ T cells in the spleen of untreated WT and *cGas*$^{-/-}$ mice (*SI Appendix*, Fig. S7*A*), *cGas*$^{-/-}$ mice showed splenomegaly on day 80 when they developed advanced colon cancer (*SI Appendix*, Fig. S1 *B* and *C*). However, the percentage of $CD3^+CD4^+$ and $CD3^+CD8^+$ T cell subsets in the spleen did not show a significant difference between WT and *cGas*$^{-/-}$ mice (*SI Appendix*, Fig. S7*B*). The populations of $CD3^+CD4^+$ and $CD3^+CD8^+$ T cells in the lamina propria were markedly higher in *cGas*$^{-/-}$ mice compared to those in WT mice on day 80 after AOM injection (Fig. 6*A*). Both $CD3^+CD4^+$ and $CD3^+CD8^+$ T cells in the colon of *cGas*$^{-/-}$ mice expressed higher levels of CD44, CD69, and PD-1 (Fig. 6 *B* and *D*), indicating more activated T cells in *cGas*$^{-/-}$ mice during CAC. However, more $CD4^+CD25^+$ T cells were also found in the colon of *cGas*$^{-/-}$ mice, suggesting an adaptive increase of regulatory T cells in response to colon inflammation. Further analysis of T cell population showed that significantly more memory $CD4^+$ and $CD8^+$ T cells but less naïve $CD4^+$ and $CD8^+$ T cells were present in the colon of *cGas*$^{-/-}$ mice (Fig. 6 *C* and *E*). $CD8^+$ T cells in tumor-bearing *cGas*$^{-/-}$ mice showed higher production of Granzyme B, but not IFN-γ (*SI Appendix*, Fig. S7*C*).

To more clearly define which cell types infiltrate into the tumors, we compared immune cells within the tumor and adjacent normal tissues. As the tumor numbers and sizes in WT mice were too small, we only performed this comparison for *cGas*$^{-/-}$ mice. Results showed that there were more $CD4^+$ and $CD8^+$ T cells infiltrating into tumors compared to adjacent normal tissues (*SI Appendix*, Fig. S7*D*). The $CD4^+$ T and $CD8^+$ T cells were mainly of the memory type (*SI Appendix*, Fig. S7*D*). However, both $CD4^+$ and $CD8^+$ T cells in tumors showed much higher PD-1 expression (*SI Appendix*, Fig. S7*E*), indicating T cell exhaustion may occur within tumors. These findings suggest that *cGas*$^{-/-}$ mice have more inflammation in the colon and maintain an immune suppressive microenvironment that may promote colon cancer growth and development.

Myeloid-Derived Suppressor Cells and Th17 Cells Accumulate in the Colon Tumors in cGAS-Deficient Mice. Higher numbers and percentages of myeloid-derived suppressor cells (MDSCs), which are known to suppress antitumor immunity, were detected in both the colon and spleen of *cGas*$^{-/-}$ mice with CAC (Fig. 7*A*). In the tumors there

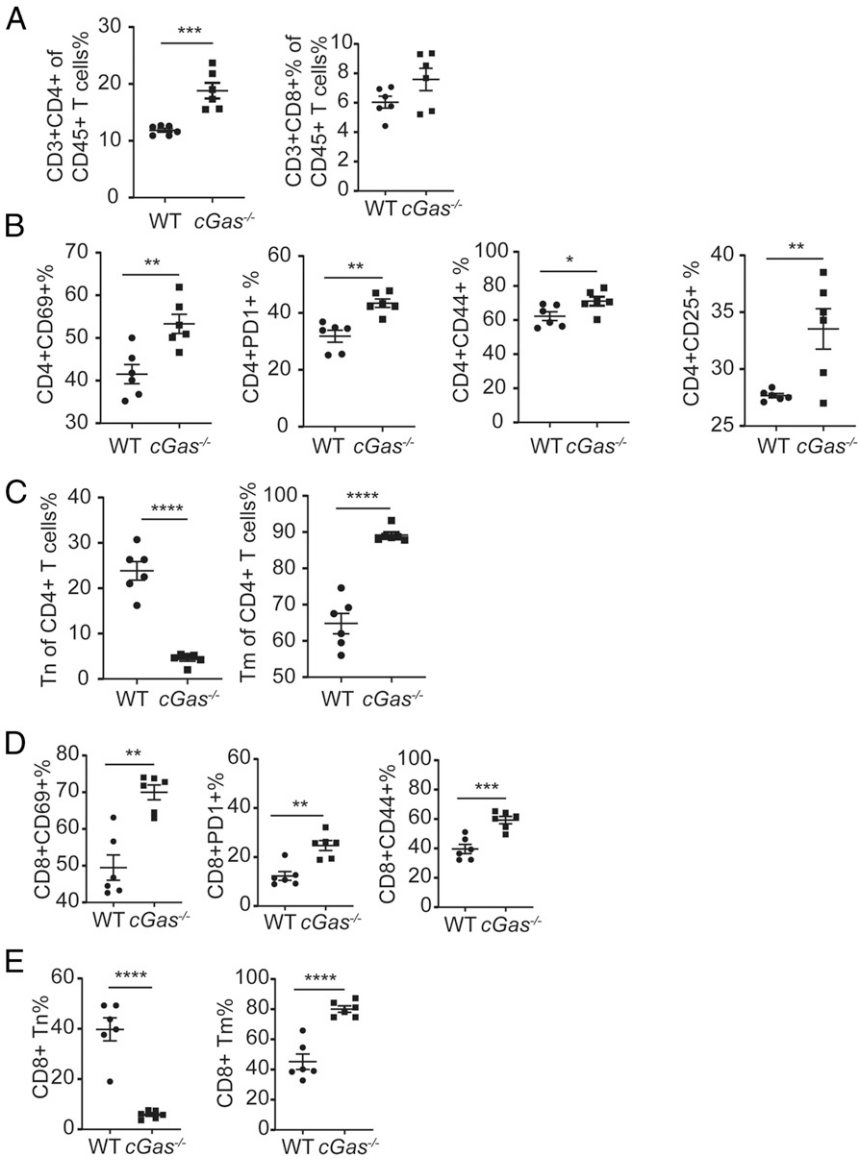

Fig. 6. Dysregulation of T cells in *cGas*$^{-/-}$ mice during colon cancer development. Mouse colon tumors were induced as described in Fig. 2. The populations of CD4^{+} and CD8^{+} T cells (*A*), activation markers in CD4 (*B*), and CD8 (*D*) T cells, and populations of naïve (CD44^{lo}CD62L^{hi}) and memory (CD44^{hi}CD62L^{lo}) CD4 (*C*) and CD8 (*E*) T cells in the lamina propria were analyzed on day 80 after AOM injection ($n = 6$ per group). *$P < 0.05$; **$P < 0.01$; ***$P < 0.001$; ****$P < 0.0001$.

were significantly higher numbers of MDSCs compared to adjacent normal tissues (*SI Appendix*, Fig. S7*F*). MDSC recruitment is regulated by chemokines, such as CXCL1 and CCL2 (36). Indeed, the expression levels of both CXCL1 and CCL2 were higher in the colon of *cGas*$^{-/-}$ mice (Fig. 7 *B* and *C*).

Recent studies have shown that the Th17 cell population promotes colonic inflammation and cancer development (37). To explore whether cGAS deficiency promotes colon inflammation and cancer development by regulating T cell activation and differentiation, we isolated colon lamina propria cells, and measured cytokine production after stimulation with Phorbol 12-myristate 13-acetate and ionomycin. Compared to WT mice, *cGas*$^{-/-}$ mice showed significantly more IL-17–producing CD4^{+} T cells and less IL-10–producing CD4^{+} T cells in the lamina propria during colon cancer development (Fig. 7*D*). However, IFN-γ–producing CD4^{+} T cells in the lamina propria were similar between WT and *cGas*$^{-/-}$ mice (Fig. 7*D*). Similar populations of IL-17– and IL-10–producing T cells were present in the colons of WT and *cGas*$^{-/-}$ mice in the untreated groups (*SI Appendix*, Fig. S7*G*). Further analysis showed that IL-17A mRNA levels were elevated in the colons of *cGas*$^{-/-}$ mice compared to WT mice on day 80 after the AOM treatment, while serum IL-17A concentrations in *cGas*$^{-/-}$ mice increased on day 15 and day 80 after the treatment (Fig. 7 *E* and *F*). Retinoid acid receptor-related orphan receptor-γ t (RORγt) is a Th17 cell differentiation lineage-specific transcription factor. Consistently, a higher percentage of RORγt^{+} population in CD3^{+}CD4^{+} T cells from the colon of *cGas*$^{-/-}$ mice was detected by flow cytometry on day 80 (Fig. 7*G*). The populations of IFN-γ–, IL-17–, and IL-10–producing CD4^{+} T cells in the spleen were similar between WT and *cGas*$^{-/-}$ mice on day 80 (*SI Appendix*, Fig. S7*H*), suggesting that cGAS deficiency promotes Th17 cell development within the colonic local environment. The *cGas*$^{-/-}$ mice developed splenomegaly, and the absolute numbers of total spleen cells, CD4^{+} T cells, CD8^{+} T cells, Th17^{+} cells and B cells in the spleen of *cGas*$^{-/-}$ mice were higher than those in the WT mice (*SI Appendix*, Fig. S7*I*). However, for DSS-induced acute colitis, although there

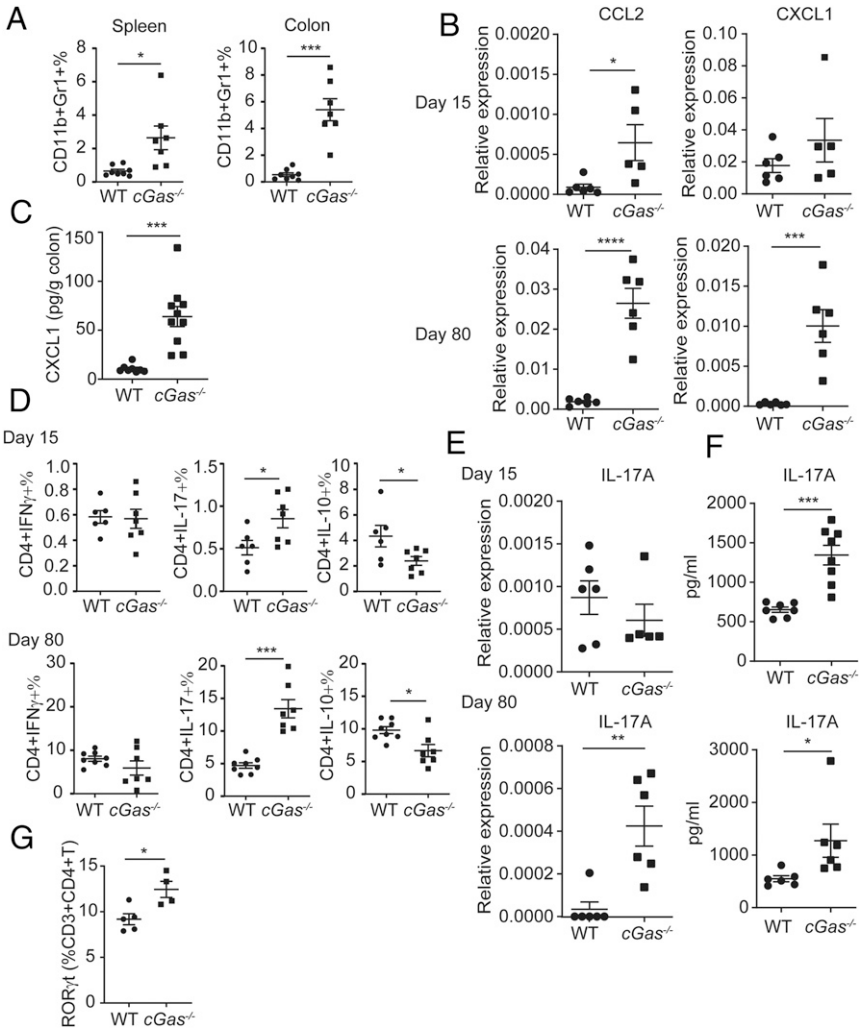

Fig. 7. Loss of cGAS promotes MDSC and Th17 cell development in colons. Mouse colon tumors were induced as described in Fig. 2. (*A*) $CD11b^+Gr1^+$ MDSC populations in the spleen and lamina propria on day 80 after AOM injection were quantified by flow cytometry. (*B*) qRT-PCR analysis of the CCL2 and CXCL1 RNA in the colon of WT and *cGas*$^{-/-}$ mice on days 15 and 80 after injection of AOM. (*C*) CXCL1 protein levels in the colon on day 80 after AOM injection were quantified by ELISA. (*D*) Percentages of $CD4^+$ T cells expressing IFN-γ, IL-10, and IL-17 in the lamina propria were quantified by flow cytometry on day 15 (WT, $n = 6$; *cGas*$^{-/-}$ mice, $n = 7$) and day 80 (WT, $n = 8$; *cGas*$^{-/-}$ mice, $n = 7$). (*E*) qRT-PCR analysis of IL-17A RNA in the colon of WT and *cGas*$^{-/-}$ mice on day 15 and 80 after injection of AOM. (*F*) IL-17A protein levels in the sera were quantified by ELISA. (*G*) The percentage of $ROR\gamma t^+$ cells in $CD3^+CD4^+$ T cells in the lamina propria on day 80 after AOM injection was quantified by flow cytometry. $^*P < 0.05$; $^{**}P < 0.01$; $^{***}P < 0.001$; $^{****}P < 0.0001$.

were higher percentages of $CD3^+CD4^+$ and $CD3^+CD8^+$ T cells in the colonic lamina propria of *cGas*$^{-/-}$ mice compared to those of WT mice on day 8 (*SI Appendix*, Fig. S7*J*), the production of IL-10, IL-17, and IFN-γ in T cells was similar between WT and *cGas*$^{-/-}$ mice (*SI Appendix*, Fig. S7*K*), suggesting that Th17 cell differentiation occurred at the later stage of the colon cancer development.

Discussion

Herein we present evidence that the absence of cGAS leads to severe colon inflammation and CAC, but not sporadic colon cancer. Surprisingly, mice lacking STING or IFNAR did not exhibit accelerated colon cancer development in the AOM/DSS model. Thus, the role of cGAS in preventing colon cancer development appears to be independent of STING or type I IFN signaling. Our results are inconsistent with other reports showing that STING deficiency promoted colon inflammation and cancer (38, 39). The reason for this discrepancy is unknown, but we noted that in the previous studies higher concentrations of DSS (3 to 5%) were used to induce colon tumors. We found that about half of the *cGas*$^{-/-}$ mice succumbed to 2.5% DSS treatment in our AOM/DSS tumor models (Fig. 2*E*). Therefore, we reduced the DSS concentration to 1.5% DSS in our experiments. Using our experimental condition (8 mg/kg AOM and three cycles of 1.5% DSS), we found that *cGas*$^{-/-}$ but not *Sting*$^{gt/gt}$ developed numerous large tumors. Our further analysis revealed that cGAS but not STING was highly expressed in the crypts including the intestinal stem cells, and that the $Lgr5^+$ stem cells decreased significantly in the *cGas*$^{-/-}$ but not *Sting*$^{gt/gt}$ mice following DSS treatment. Supporting these results, *cGas*$^{-/-}$ but not *Sting*$^{gt/gt}$ mice exhibited impaired gut barrier function as evidenced by the leakage of FITC-dextran from the gut lumen to the blood. These results suggest that cGAS protects the integrity of the gut barrier through a STING-independent mechanism, likely by regulating stem cell function and tissue repair.

Colorectal cancer is among the cancer types that acquire the most mutation burden. Accumulation of driver mutations via both genetic and epigenetic mechanisms is thought to promote colorectal tumorigenesis. cGAS senses genomic instability and DNA damage to promote cell death and clearance (16–18, 40). Recent studies show that a substantial fraction of cGAS is tethered to the

chromatin, and chromatin-associated cGAS may directly regulate DNA repair in a STING-independent manner (41–44). Therefore, it is possible that loss of cGAS may result in elevated genomic instability in colorectal tissues that promotes cancer development. Our data suggest that the STING-independent mechanism serves an important role in the function of cGAS in controlling colorectal tumorigenesis, although STING-dependent function of cGAS in other cell types may also be important (20, 45). Interestingly, epigenetic silencing of cGAS gene expression has been frequently found in human colorectal carcinoma cell lines (46).

cGAS-deficient mice did not display defects in the production of type I IFNs but rather produced more inflammatory cytokines and chemokines, including IL-6, IL-1β, CCL2, and CXCL1. The enhanced production of these inflammatory mediators is likely due to the impairment of the intestinal barrier in the *cGas*$^{-/-}$ mice. The increased permeability of the intestinal barrier and the loss of the mucin layer in the *cGas*$^{-/-}$ mice likely lead to enhanced inflammation in the colonic tissues, which is evident by increased expression of IL-6, IL-1β, and MIP2, and the resultant activation of STAT3. Increased activity of STAT3 is common in human malignancies, including primary human colorectal cancers and established human colorectal cancer cell lines (47). STAT3 activation may lead to more colonic epithelial proliferation, which was evident in cGAS-deficient mice. Inhibition of STAT3 with a chemical inhibitor led to partial reduction of tumor numbers in the *cGas*$^{-/-}$ mice. Interestingly, cGAS-deficient mice showed more epithelial proliferation but also more apoptosis during CAC, especially within the tumors. The death of the IECs of *cGas*$^{-/-}$ mice may lead to the defect of the epithelial barrier, exacerbating inflammation. This vicious cycle of cell death, inflammation, and proliferation may underlie the development of colitis associated colon cancer.

The inflammatory environment in the tumors not only promotes proliferation of tumor cells, but also leads to recruitment of MDSCs through chemokines, such as CCL2 and CXCL1, which are highly induced in *cGas*$^{-/-}$ mice. Furthermore, the inflammatory mediators, IL-6 and IL-1β, promote the development of Th17 cells in the colon, which together with MDSCs form an immune suppressive microenvironment that is conducive to tumor growth and evasion from the immune system. In addition, higher PD-1 expression in the $CD4^+$ and $CD8^+$ T cells in the tumors of *cGas*$^{-/-}$ mice indicates the exhaustion status of T cells in the tumor microenvironment that could also suppresses antitumor immunity.

Colon cancers are known to be highly refractory to immunotherapy, including immune checkpoint inhibitors, such as antibodies against PD-1 and PD-L1. Stimulation of innate immunity, such as the use of STING agonists, has been shown to be highly effective in mouse tumor models in part by inducing type I IFNs and changing the tumor microenvironments to facilitate the recruitment of T cells and natural killer cells. However, the therapeutic effects of STING agonists have only been shown in mouse models bearing transplanted tumor cell lines. We found that intraperitoneal delivery of cGAMP to *cGas*$^{-/-}$ mice that harbor colon tumors led to a reduction of the tumor numbers in the colons, providing evidence that STING agonists are effective in treating tumors arising from endogenous tissues. Although *Sting*$^{gt/gt}$ mice did not phenocopy *cGas*$^{-/-}$ mice in colon cancer development, activation of STING in the *cGas*$^{-/-}$ mice with cGAMP can still exert antitumor effects by activating the innate immune system such as induction of type-I interferons.

Materials and Methods

Detailed descriptions are provided in *SI Appendix*.

Mice. *cGas*$^{-/-}$ mice were generated as previously reported (48). WT C57BL/6J, B6.SJL-*Ptprc*^{a} *Pepc*^{b}/BoyJ, B6(Cg)-*Sting1tm1.2Camb*/J, C57BL/6J-*Sting1gt*/J and Lgr5-EGFP-IRES-creERT2 mice were purchased from the Jackson Laboratory. The *Apc(min/+)* and *IFNAR*$^{-/-}$ mice were kindly provided, respectively, by Joshua Mendell and David Farrar, University of Texas Southwestern, Dallas, TX. All of these strains were maintained on C57BL6/J background and bred in a specific pathogen-free facility. To rule out the contribution of microbiota in influencing colon inflammation and cancer development, WT and *cGas*$^{-/-}$ mice were cohoused for at least 2 wk for all experiments; in some cases, where indicated, the mice were cohoused throughout the duration of the experiments. All study protocols were approved by the Institutional Care and Use Committee of the University of Texas Southwestern Medical Center and were conducted in accordance with the Institutional Animal Care and Use Committee guidelines and the NIH *Guide for the Care and Use of Laboratory Animals* (49). All the experiments were conducted with sex and age-matched mice and both male and female mice were included.

Induction of Tumors. To induce CAC, mice were injected intraperitoneally with 8 mg of the mutagen AOM (Sigma-Aldrich) per kilogram body weight followed by three cycles of 1.5% or indicated concentration of DSS in drinking water for 5 d, with regular drinking water for 14 d between each cycle. Mice were euthanized on day 80 or when moribund. For day 15 samples, mice were injected with AOM, and after 5 d, they were fed with DSS for 5 d. Mice were then fed with regular water for 5 d before experimental analyses.

Processing of scRNA-Seq Data. The epithelial cell dataset (GSE92332) was loaded to Seurat v3 (26, 50). Data were transformed to $\log_2$(TPM+1) (TPM, transcripts per million) and scaled in Seurat. Principal components analysis was calculated based on top 2,000 variable features. Cells were plotted by t-distributed stochastic neighbor embedding (t-SNE) method and cell types were labeled based on the original annotations of ref. 26. scRNA-seq datasets from whole epithelium and enriched crypts (GSE123516) were read into Seurat and filtered based on the proportion of mitochondrial genes (percent.mt < 50) (27). Data were log-normalized and scaled in the Seurat. The resolution for cell clustering is based on the original paper. Cell types were labeled based on the gene-expression pattern shown in the Extended Data of ref. 27.

Statistical Analysis. Data were analyzed by Prism7 (GraphPad Software) and statistical significance was determined by two-tailed Student *t* test unless specifically defined otherwise. $P < 0.05$ was considered statistically significant.

Data Availability. All study data are included in the article and *SI Appendix*.

ACKNOWLEDGMENTS. This work was supported by grants from the National Cancer Institute (U54CA244719), Welch Foundation (I-1389), and Cancer Prevention and Research Institute of Texas (RP180725). Z.J.C. is an investigator of the HHMI.

1. R. L. Siegel, K. D. Miller, A. Jemal, Cancer statistics, 2019. *CA Cancer J. Clin.* **69**, 7–34 (2019).
2. R. Francescone, V. Hou, S. I. Grivennikov, Cytokines, IBD, and colitis-associated cancer. *Inflamm. Bowel Dis.* **21**, 409–418 (2015).
3. M. Saleh, G. Trinchieri, Innate immune mechanisms of colitis and colitis-associated colorectal cancer. *Nat. Rev. Immunol.* **11**, 9–20 (2011).
4. L. Sun, J. Wu, F. Du, X. Chen, Z. J. Chen, Cyclic GMP-AMP synthase is a cytosolic DNA sensor that activates the type I interferon pathway. *Science* **339**, 786–791 (2013).
5. J. Wu *et al.*, Cyclic GMP-AMP is an endogenous second messenger in innate immune signaling by cytosolic DNA. *Science* **339**, 826–830 (2013).
6. A. Ablasser, Z. J. Chen, cGAS in action: Expanding roles in immunity and inflammation. *Science* **363**, eaat8657 (2019).
7. Q. Chen, L. Sun, Z. J. Chen, Regulation and function of the cGAS-STING pathway of cytosolic DNA sensing. *Nat. Immunol.* **17**, 1142–1149 (2016).
8. S. R. Woo *et al.*, STING-dependent cytosolic DNA sensing mediates innate immune recognition of immunogenic tumors. *Immunity* **41**, 830–842 (2014).
9. G. N. Barber, STING: Infection, inflammation and cancer. *Nat. Rev. Immunol.* **15**, 760–770 (2015).
10. L. Deng *et al.*, STING-dependent cytosolic DNA sensing promotes radiation-induced type I interferon-dependent antitumor immunity in immunogenic tumors. *Immunity* **41**, 843–852 (2014).
11. R. M. Chabanon *et al.*, PARP inhibition enhances tumor cell-intrinsic immunity in ERCC1-deficient non-small cell lung cancer. *J. Clin. Invest.* **129**, 1211–1228 (2019).
12. H. Wang *et al.*, cGAS is essential for the antitumor effect of immune checkpoint blockade. *Proc. Natl. Acad. Sci. U.S.A.* **114**, 1637–1642 (2017).
13. C. Zierhut *et al.*, The cytoplasmic DNA sensor cGAS promotes mitotic cell death. *Cell* **178**, 302–315.e23 (2019).
14. M. M. Xu *et al.*, Dendritic cells but not macrophages sense tumor mitochondrial DNA for cross-priming through signal regulatory protein α signaling. *Immunity* **47**, 363–373.e5 (2017).
15. Z. Dou *et al.*, Cytoplasmic chromatin triggers inflammation in senescence and cancer. *Nature* **550**, 402–406 (2017).

16. S. Glück *et al*., Innate immune sensing of cytosolic chromatin fragments through cGAS promotes senescence. *Nat. Cell Biol.* **19**, 1061–1070 (2017).
17. T. Li, Z. J. Chen, The cGAS-cGAMP-STING pathway connects DNA damage to inflammation, senescence, and cancer. *J. Exp. Med.* **215**, 1287–1299 (2018).
18. H. Yang, H. Wang, J. Ren, Q. Chen, Z. J. Chen, cGAS is essential for cellular senescence. *Proc. Natl. Acad. Sci. U.S.A.* **114**, E4612–E4620 (2017).
19. S. F. Bakhoum *et al*., Chromosomal instability drives metastasis through a cytosolic DNA response. *Nature* **553**, 467–472 (2018).
20. Q. Chen *et al*., Carcinoma-astrocyte gap junctions promote brain metastasis by cGAMP transfer. *Nature* **533**, 493–498 (2016).
21. J. Nassour *et al*., Autophagic cell death restricts chromosomal instability during replicative crisis. *Nature* **565**, 659–663 (2019).
22. S. Wirtz *et al*., Chemically induced mouse models of acute and chronic intestinal inflammation. *Nat. Protoc.* **12**, 1295–1309 (2017).
23. C. Neufert, C. Becker, M. F. Neurath, An inducible mouse model of colon carcinogenesis for the analysis of sporadic and inflammation-driven tumor progression. *Nat. Protoc.* **2**, 1998–2004 (2007).
24. T. Tanaka *et al*., A novel inflammation-related mouse colon carcinogenesis model induced by azoxymethane and dextran sodium sulfate. *Cancer Sci.* **94**, 965–973 (2003).
25. A. R. Moser, H. C. Pitot, W. F. Dove, A dominant mutation that predisposes to multiple intestinal neoplasia in the mouse. *Science* **247**, 322–324 (1990).
26. A. L. Haber *et al*., A single-cell survey of the small intestinal epithelium. *Nature* **551**, 333–339 (2017).
27. A. Ayyaz *et al*., Single-cell transcriptomes of the regenerating intestine reveal a revival stem cell. *Nature* **569**, 121–125 (2019).
28. A. R. Bresnick, D. J. Weber, D. B. Zimmer, S100 proteins in cancer. *Nat. Rev. Cancer* **15**, 96–109 (2015).
29. M. F. Neurath, Current and emerging therapeutic targets for IBD. *Nat. Rev. Gastroenterol. Hepatol.* **14**, 269–278 (2017).
30. S. Grivennikov *et al*., IL-6 and Stat3 are required for survival of intestinal epithelial cells and development of colitis-associated cancer. *Cancer Cell* **15**, 103–113 (2009).
31. S. I. Grivennikov *et al*., Adenoma-linked barrier defects and microbial products drive IL-23/IL-17-mediated tumour growth. *Nature* **491**, 254–258 (2012).
32. X. Xu *et al*., Chemical probes that competitively and selectively inhibit Stat3 activation. *PLoS ONE* **4**, e4783 (2009).
33. I. C. Allen *et al*., The NLRP3 inflammasome functions as a negative regulator of tumorigenesis during colitis-associated cancer. *J. Exp. Med.* **207**, 1045–1056 (2010).
34. J. E. Wilson *et al*., Inflammasome-independent role of AIM2 in suppressing colon tumorigenesis via DNA-PK and Akt. *Nat. Med.* **21**, 906–913 (2015).
35. S. Hu *et al*., The DNA sensor AIM2 maintains intestinal homeostasis via regulation of epithelial antimicrobial host defense. *Cell Rep.* **13**, 1922–1936 (2015).
36. H. Katoh *et al*., CXCR2-expressing myeloid-derived suppressor cells are essential to promote colitis-associated tumorigenesis. *Cancer Cell* **24**, 631–644 (2013).
37. M. Tosolini *et al*., Clinical impact of different classes of infiltrating T cytotoxic and helper cells (Th1, th2, treg, th17) in patients with colorectal cancer. *Cancer Res.* **71**, 1263–1271 (2011).
38. Q. Zhu *et al*., Cutting edge: STING mediates protection against colorectal tumorigenesis by governing the magnitude of intestinal inflammation. *J. Immunol.* **193**, 4779–4782 (2014).
39. J. Ahn, S. Son, S. C. Oliveira, G. N. Barber, STING-dependent signaling underlies IL-10 controlled inflammatory colitis. *Cell Rep.* **21**, 3873–3884 (2017).
40. B. Larkin *et al*., Cutting edge: Activation of STING in T cells induces type I IFN responses and cell death. *J. Immunol.* **199**, 397–402 (2017).
41. H. Jiang *et al*., Chromatin-bound cGAS is an inhibitor of DNA repair and hence accelerates genome destabilization and cell death. *EMBO J.* **38**, e102718 (2019).
42. H. Liu *et al*., Nuclear cGAS suppresses DNA repair and promotes tumorigenesis. *Nature* **563**, 131–136 (2018).
43. H. E. Volkman, S. Cambier, E. E. Gray, D. B. Stetson, Tight nuclear tethering of cGAS is essential for preventing autoreactivity. *eLife* **8**, e47491 (2019).
44. H. Chen *et al*., cGAS suppresses genomic instability as a decelerator of replication forks. *Sci. Adv.* **6**, eabb8941 (2020).
45. J. Ahn *et al*., Inflammation-driven carcinogenesis is mediated through STING. *Nat. Commun.* **5**, 5166 (2014).
46. T. Xia, H. Konno, J. Ahn, G. N. Barber, Deregulation of STING signaling in colorectal carcinoma constrains DNA damage responses and correlates with tumorigenesis. *Cell Rep.* **14**, 282–297 (2016).
47. F. M. Corvinus *et al*., Persistent STAT3 activation in colon cancer is associated with enhanced cell proliferation and tumor growth. *Neoplasia* **7**, 545–555 (2005).
48. X. D. Li *et al*., Pivotal roles of cGAS-cGAMP signaling in antiviral defense and immune adjuvant effects. *Science* **341**, 1390–1394 (2013).
49. National Research Council, *Guide for the Care and Use of Laboratory Animals* (National Academies Press, Washington, DC, ed. 8, 2011).
50. A. Butler, P. Hoffman, P. Smibert, E. Papalexi, R. Satija, Integrating single-cell transcriptomic data across different conditions, technologies, and species. *Nat. Biotechnol.* **36**, 411–420 (2018).